BBA - Molecular Basis of Disease 1865 (2019) 2257–2266

Contents lists available at ScienceDirect

BBA - Molecular Basis of Disease

journal homepage: www.elsevier.com/locate/bbadis

Missense variant in *TPI1* (Arg189Gln) causes neurologic deficits through structural changes in the triosephosphate isomerase catalytic site and reduced enzyme levels in vivo

Bartholomew P. Roland[a,b,c], Kristen R. Richards[g], Stacy L. Hrizo[a,b,h], Samantha Eicher[a,b], Zackery J. Barile[a,b], Tien-Chien Chang[a,b], Grace Savon[a,b], Paola Bianchi[d], Elisa Fermo[d], Bianca Maria Ricerca[e], Luca Tortorolo[f], Jerry Vockley[i], Andrew P. VanDemark[g,*], Michael J. Palladino[a,b,*]

[a] Department of Pharmacology & Chemical Biology, University of Pittsburgh School of Medicine, Pittsburgh, PA 15261, USA
[b] Pittsburgh Institute for Neurodegenerative Diseases (PIND), University of Pittsburgh School of Medicine, Pittsburgh, PA 15261, USA
[c] Department of Pharmacology, Vanderbilt University, Nashville, TN 37232, USA
[d] Fondazione IRCCS Ca' Granda Ospedale Maggiore Policlinico, UOC Ematologia, UOS Fisiopatologia delle Anemie, Via F Sforza, 35, 20122 Milan, Italy
[e] Hematology Institute, Universitary Hospital A. Gemelli, Largo A. Gemelli 8, 00168 Rome, Italy
[f] Pediatric Intensive Care Unit, Universitary Hospital A. Gemelli, Largo A. Gemelli 8, 00168 Rome, Italy
[g] Biological Sciences and Structural Biology, University of Pittsburgh, Pittsburgh, PA 15260, USA
[h] Department of Biology, Slippery Rock University, Slippery Rock, PA 16057, USA
[i] Department of Pediatrics and Human Genetics, University of Pittsburgh Schools of Medicine and Public health, Pittsburgh, PA 15261, USA

ARTICLE INFO

Keywords:
Triosephosphate isomerase
TPI deficiency
Glycolytic enzymopathy
Genomic engineering

ABSTRACT

Mutations in the gene *triosephosphate isomerase* (*TPI*) lead to a severe multisystem condition that is characterized by hemolytic anemia, a weakened immune system, and significant neurologic symptoms such as seizures, distal neuropathy, and intellectual disability. No effective therapy is available. Here we report a compound heterozygous patient with a novel TPI pathogenic variant (NM_000365.5:c.569G > A:p.(Arg189Gln)) in combination with the common (NM_000365.5:c.315G > C:p.(Glu104Asp)) allele. We characterized the novel variant by mutating the homologous Arg in *Drosophila* using a genomic engineering system, demonstrating that missense mutations at this position cause a strong loss of function. Compound heterozygote animals were generated and exhibit motor behavioural deficits and markedly reduced protein levels. Furthermore, examinations of the $TPI^{Arg189Gln}/TPI^{Glu104Asp}$ patient fibroblasts confirmed the reduction of TPI levels, suggesting that Arg189Gln may also affect the stability of the protein. The Arg189 residue participates in two salt bridges on the backside of the TPI enzyme dimer, and we reveal that a mutation at this position alters the coordination of the substrate-binding site and important catalytic residues. Collectively, these data reveal a new human pathogenic variant associated with TPI deficiency, identify the Arg189 salt bridge as critical for organizing the catalytic site of the TPI enzyme, and demonstrates that reduced TPI levels are associated with human TPI deficiency. These findings advance our understanding of the molecular pathogenesis of the disease, and suggest new therapeutic avenues for pre-clinical trials.

1. Introduction

Triosephosphate isomerase (TPI) is a glycolytic enzyme that converts dihydroxyacetone phosphate (DHAP) into glyceraldehyde 3-phosphate (GAP). The isomerization of these two metabolites doubles the efficiency of glycolysis, though it is not an obligate step for glycolytic flux. Dysfunction within the human *TPI* gene causes an autosomal recessive disease known as TPI deficiency [1]. TPI deficiency is part of a larger family of diseases known as glycolytic enzymopathies. These disorders are caused by dysfunction of various proteins within the glycolytic pathway and typically lead to hemolytic anemia; however, TPI deficiency has also been shown to lead to neurologic symptoms [2–5]. A common pathogenic mutation has been identified in patients with TPI deficiency (TPI^{E104D}), while TPI^{C41Y}, TPI^{A62D}, TPI^{I170V},

* Corresponding authors at: University of Pittsburgh, Pittsburgh, PA, USA.
E-mail addresses: andyv@pitt.edu (A.P. VanDemark), mjp44@pitt.edu (M.J. Palladino).

https://doi.org/10.1016/j.bbadis.2019.05.002
Received 23 February 2018; Received in revised form 20 December 2018; Accepted 6 January 2019
Available online 07 May 2019
0925-4439/

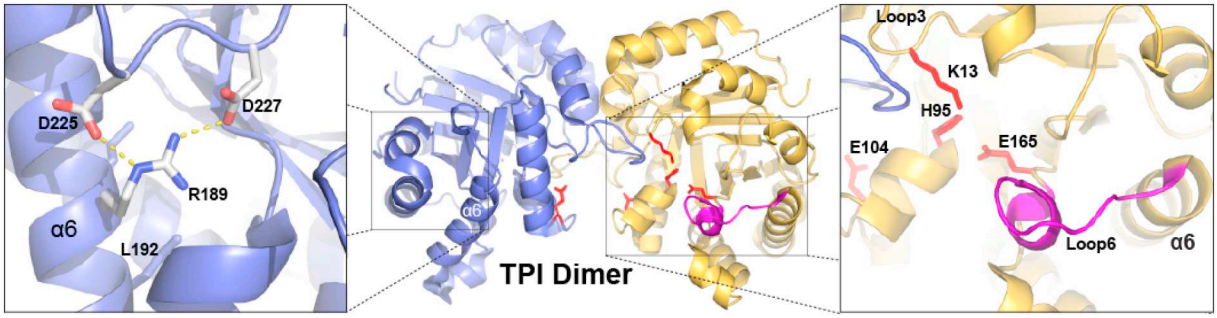

Fig. 1. Wild type human TPI protein structure. Human TPI exists as a dimer (center) and its structure is shown here with one monomer in gold and one in blue. The left inset shows the R189 salt bridge with D225 and D227 at the distal end of the TPI dimer, while the right inset shows the key catalytic residues K13, H95, and E165. These catalytic residues are shown juxtaposed next to important components of the TPI dimer interface, Loop3 and E104. PDB ID: 4POC. (For interpretation of the references to colour in this figure legend, the reader is referred to the web version of this article.)

TPI^{V231M}, and *TPI*^{F240L} have also been associated with the disease [6–11]. *TPI* mutations produce a spectrum of clinical symptoms in patients, raising questions about penetrance and expressivity. In one noteworthy report, two identical twins with the same *TPI* genotype had dramatically different health outcomes; one brother exhibited severe distal weakness and hemolytic anemia, while the other showed hemolytic anemia only [11]. These clinical observations demonstrate that environmental or genetic modifiers can modulate the disease.

TPI functions as a homodimer, with each monomer containing an independent catalytic site nested at the top of a $(\beta\alpha)_8$ barrel structure known as a triose isomerase (TIM) barrel. Loop3 of the TPI monomer reciprocally extends into its dimer partner, and forms the bulk of the dimer interface (Fig. 1). Mutations along this dimer interface have been shown to severely impair the stability of the TPI dimer [12]. Loop6 of the TPI monomer forms the catalytic lid of the enzyme, and its movements dictate accessibility of the substrate to the catalytic site (Fig. 1). Substrate isomerization is coordinated by three key catalytic residues, K13, H95, and E165 [13]. E165 has been shown to swing in and out of the catalytic pocket ~2 Å in a planar motion, and when swung in, this residue is capable of abstracting and transferring a proton from the C1 to the C2 position of its DHAP substrate [14]. K13 and N95 of the catalytic site stabilize the enediolate intermediate during this transfer, and the closure/hydrogen bonding of Loop6 excludes water from entering the pocket [13]. The exclusion of water is particularly critical for preventing the phosphate elimination reaction, which will occur readily in solution, forming the toxic byproduct methylglyoxal. Mutations of Loop6 or its surrounding hinge residues have been shown to slow the catalytic cycle of TPI [15–17]. It is believed that the closure and reopening of the enzyme lid, followed by substrate diffusion, are the key rate-limiting steps of the enzyme.

Three crystal structures of human disease-associated *TPI* mutations have revealed that defects in enzyme dimerization and catalytic activity are sufficient to cause TPI deficiency [18–20]. The pathogenic *TPI*^{E104D} mutation sits at the dimer interface of these TIM barrels, perturbs dimer formation, and reduces protein stability (Fig. 1) [19]. Conversely, the *TPI*^{I170V} and *TPI*^{V231M} mutations interfere with catalytic activity, rather than reducing dimerization [18,20]. I170 is part of Loop6, the lid of the catalytic site, and alterations of this aliphatic residue are sufficient to change the hydrogen bonding properties within the catalytic site [20]. V231 sits on the floor of the catalytic site, and the mutation to a methionine at this position will shift the peptide backbone of α8 into the substrate-binding pocket [18]. These three molecular sources of pathogenesis are structurally distinct, but enzymatically related. Catalytic activity of the enzyme is supported by TPI dimerization, and monomeric TPI is predicted to be unstable and likely rapidly degraded [12]. Mutant TPI protein degradation can be attenuated by inhibiting the proteasome, and indeed this ameliorates neurologic dysfunction and early death of a TPI dimer mutation in *Drosophila* [21]. Thus, understanding the molecular dysfunction associated with each mutation may help target individual therapeutic strategies.

The present study outlines the clinical profile of a patient with two different mutant *TPI* alleles, (NM_000365.5:c.569G > A:p.(R189Q)) and (NM_000365.5:c.315G > C:p.(E104D)). The molecular dysfunction associated with *TPI*^{E104D} has been shown to be caused by impaired homodimerization, resulting in altered affinity for substrate and reduced thermal stability [18,19]. However, *TPI*^{R189Q} has not previously been described in a TPI deficiency patient (ClinVar accession number SCV000882820). This arginine acts as the basic partner of two acidic aspartates (D225 and D227), and together form an important determinant of protein stability by tethering the C terminus of the 7th and 8th folds of the beta barrel to the rest of the protein (Fig. 1). Mutations that alter the charge or hydrophilicity at either of the R189 and D227 positions can also impair protein folding [22]. Based on these observations, we introduced similar structural mutations into the homologous *TPI* position of *Drosophila* to evaluate whether these alterations were sufficient to induce pathology. Our findings indicate that mutations in this conserved salt bridge are sufficient to reduce protein stability and elicit TPI deficiency pathogenesis, supporting the need for therapeutic interventions aimed at supporting TPI protein stability and reduced enzyme turnover.

2. Results

2.1. Clinical history

The propositus was an Italian girl, the first child of non-consanguineous parents, born at 37 weeks gestation after an uneventful pregnancy. Neonatal jaundice was present requiring phototherapy. At 3 weeks of age during a probable viral intercurrent illness, she developed severe anemia (Hb 6 g/dL) and received a blood transfusion. Neuromuscular impairment with respiratory deficiency was apparent at 1 month of age, and at 3 months bilateral diaframatic paralysis was diagnosed. A tracheostomy was performed at 5 months, with subsequent 24 h mechanical ventilation. The patient's clinical course was characterized by recurrent infections with haemolytic crises requiring blood transfusions, and her overall neurological condition worsened after a viral infection at 1 year of age. Brain MRI at that time showed cerebral atrophy and periventricular leukomalacia. A progressive ventilator weaning program was implemented, and by age 2 years 10 months she only required night time ventilation. Currently, the patient is 4 years and 8 months of age and remains on night ventilation with intermittent daytime support as needed with significant intellectual and neuromuscular impairment. The severe anemia initially presented following infection, and persisted after the infection was resolved. At that time, the haemoglobin level in the proband was 8.8 g/dL. Infant anemia can be caused by a spectrum of factors, including infections, immune system disorders, or hereditary diseases [23]. The sustained anemia combined with progressive neuromuscular

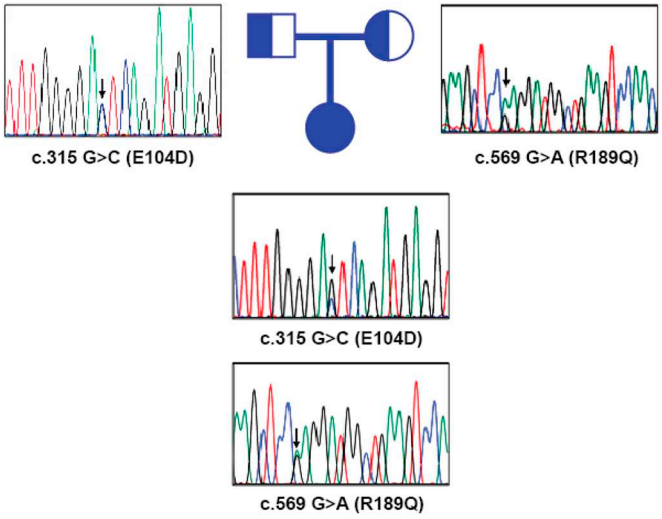

Fig. 2. Pedigree analysis of proband and parents reveals the inheritance of two different missense mutations in the *TPI1* gene. DNA samples were collected from proband and parents, and the *TPI1* gene was sequenced. A is traced in green, G is traced in black, C is traced in blue, and T is traced in red. Mixed peaks were identified at c.315G > C and c.569 G > A, in the father and mother, respectively. These affect codons resulting in E104D and R189Q amino acid substitutions, respectively. The patient inherited both of these mutations and is thus a *trans*- or compound- heterozygote. (For interpretation of the references to colour in this figure legend, the reader is referred to the web version of this article.)

indications suggested the possibility of a hereditary condition.

2.2. Molecular and enzyme studies

Molecular testing for genes of glycolytic disorders identified two missense mutations in the TPI coding region: c.315 G > C (p.E104D) and the new variant c.569 G > A (p.R189Q) (Fig. 2). This numbering uses the established nomenclature for TPI mutations, assuming the start methionine is removed following translation [24]; and for consistency all residue numbering in this study uses the same convention. Sequencing of parents *TPI1* gene revealed they were each heterozygous for one of the mutations (Fig. 2). The TPI^{E104D} mutation is the most prevalent *TPI* missense mutation identified and leads to TPI deficiency in homozygous patients or in compound heterozygotes when paired with a second *TPI* mutation [8,25]. Database searches of the Human Gene Mutation Database, the 1000 Genomes, and ExAC databases did not identify the TPI^{R189Q} mutation, yet the protein prediction tools Predict SNP [26] and M-CAP [27] suggested that it is likely to be pathogenic. TPI activity from red blood cells was markedly reduced (289 UI/g Hb; reference range 1407–2133), whereas the parents displayed intermediate activity compatible with the heterozygous state (father 1446 UI/g Hb, mother 584 UI/g Hb). Collectively, these findings strongly suggest that the TPI^{R189Q} mutation is a loss-of-function allele capable of eliciting TPI deficiency.

2.3. TPI^{R189} mutations recapitulate neurologic dysfunction in animal models

To confirm the pathogenicity of the TPI^{R189} mutant allele, we utilized a genomic engineering (GE) strategy in *D. melanogaster*. We have previously created a GE system to evaluate modifications of *TPI* [28], and have since used this system to evaluate molecular determinants of TPI deficiency [20,28,29]. R189 is a conserved residue TPI, and we mutated the homologous position in the *TPI* gene of *Drosophila* (TPI^{R187}) (Fig. 3A). The *Drosophila* TPI^{R187A}, TPI^{R187K}, TPI^{R187L}, and TPI^{R187S} alleles were designed to examine the molecular determinants of TPI^{R187} dysfunction in vivo, and were generated using the *TPI* genomic engineering system outlined previously [28]. The TPI^{R187A}, TPI^{R187L}, and TPI^{R187S} alleles proved to be homozygous lethal and were maintained with balancer chromosomes, while TPI^{R187K} homozygotes were viable and capable of propagating a stable stock. These results demonstrate that alterations of the basic charge at position R187 are sufficient to elicit a strong loss-of-function.

The patient's heterozygous *TPI* genotype suggested that the TPI^{R189Q} allele was interacting with TPI^{E104D} to lead to TPI deficiency. We tested whether TPI^{R187} mutations were sufficient to elicit TPI deficiency using a complementation test with the pathogenic *Drosophila* TPI allele, TPI^{M80T}. A Met-to-Thr mutation at position 80 of *Drosophila* TPI (also called $TPI^{sugarkill}$ [30] and TPI^{wstd} [31]) is located at the enzyme dimer interface, similar to the human mutation TPI^{E104D}. TPI^{M80T} is a recessive mutation that leads to progressive neurologic defects in homozygotes, and demonstrates a similarly severe phenotype in combination with the null allele TPI^{JS10}, an allele with a 1.6 kb deletion of two of its exons (also known as TPI^{null}) [30,32]. We crossed the TPI^{R187} and TPI^{M80T} mutant flies and measured complementation of the TPI^{M80T} behavioural dysfunction (Fig. 3B). The TPI^{R187K} allele was capable of complementing the mechanical stress sensitivity of TPI^{M80T} and TPI^{null} (Fig. 3B). Conversely, TPI^{R187A}, TPI^{R187L}, and TPI^{R187S} failed to complement TPI^{M80T}, and in fact exacerbated the mechanical stress sensitivity relative to $TPI^{M80T/M80T}$(Fig. 3B). These data suggest that *TPI* alleles encoding a non-basic amino acid at residue 187 interact with TPI^{M80T} similarly to TPI^{null} [30].

Non-basic R187 mutations reduce TPI protein levels in Drosophila and patient fibroblasts.

TPI protein levels are an important determinant of pathogenesis in TPI deficiency. Mutations at the dimer interface have been shown to lead to protein degradation, and pharmacological or genetic inhibition of the protein turnover via the proteasome is capable of ameliorating behavioural dysfunction in *Drosophila* models of TPI deficiency [21,32]. Thus, we sought to determine whether the R187 substitutions altered protein levels in vivo. We crossed the TPI^{R187} alleles with an allele of TPI bearing a cyan fluorescent protein (CFP) tag, $TPI^{WT\text{-}CFP}$, to measure the protein produced by mutations in TPI^{R187}. The addition of the CFP tag to a WT allele facilitated the discrimination of the two protein products based on molecular weight, while still supporting animal viability. Lysates from animals revealed that the TPI^{R187A}, TPI^{R187L}, and TPI^{R187S} mutations reduced TPI protein levels to a greater extent than the dimer mutation TPI^{M80T} (Fig. 4A, B). In contrast, the TPI^{R187K} protein was present at a level equivalent to TPI^{WT} (Fig. 4A, B). These data demonstrate that non-basic substitutions at TPI^{R187} lead to reduced protein levels in vivo. Finally, none of the R187 substitutions significantly reduced $TPI^{WT\text{-}CFP}$ levels, though the TPI^{R187L} did seem to elicit a slight reduction (~25%) in $TPI^{WT\text{-}CFP}$ (Fig. 4C).

The R189 residue in human TPI is conserved in eukaryotes and prokaryotes (Fig. 3A), suggesting that it may have a conserved role in protein folding or stability. The mutational analysis in *Drosophila* demonstrated that non-basic substitutions contribute to reduced protein in vivo, leading us to hypothesize that the TPI^{E104D}/TPI^{R189Q} patient may also exhibit reduced levels of TPI. We collected fibroblast samples from the proband and a healthy control, and probed them for TPI protein levels (Fig. 5). TPI enzyme levels were reduced ~75% of that from the unaffected control (Fig. 5). The TPI deficient patient is a compound-heterozygote, and although we were unable to differentiate between TPI^{E104D} and TPI^{R189Q} variants, we believe > 50% reduction in TPI suggests that TPI^{R189Q} is influencing the folding or stability of TPI in the patient.

2.4. TPI^{R189} influences protein stability without altering dimerization

Previous studies have demonstrated that TPI folding defects are capable of inducing TPI deficiency [18,19,29]. Mutagenesis of residues crucial for homodimer stabilization have profound neuropathologic

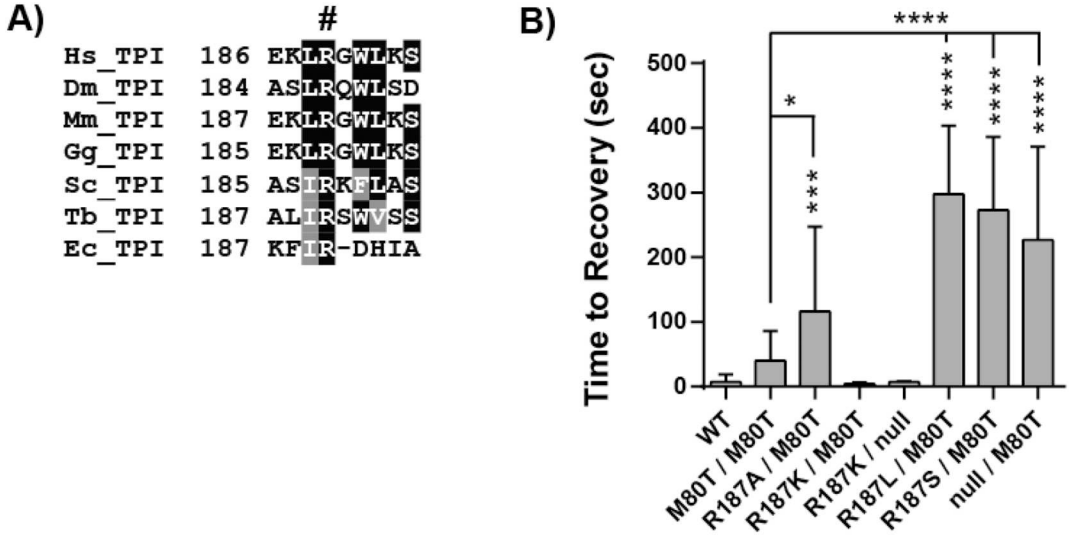

Fig. 3. Mutations of TPI^{R187} in *Drosophila* are sufficient to elicit neurologic dysfunction associated with TPI deficiency. A) Boxshade alignment of the region surrounding the human R189 residue (indicated with #). Sequence accession numbers are listed in the Materials and Methods. B) Animals heterozygous for M80 T, paired with mutations affecting the *Drosophila* R187 residue that alter its basic charge elicit mechanical stress sensitivity. Animals were reared at 25 °C and tested on day 3, n ≥ 20 animals, maximum responses capped at 360 s. Variance in data was tested with a one-way ANOVA, comparisons between groups made with Tukey's post hoc test. * indicates $p < 0.05$, *** $p < 0.001$, **** $p < 0.0001$.

effects in *Drosophila melanogaster* [28,29]. In addition to the dimer interface, the conserved R189 – D225/D227 salt bridge is a known modulator of TPI stability and function in *Trypanosoma brucei* (5). R189 and D225/D227 are located in helix 6 and in the C-terminal end of helix 7, respectively; linking the C-terminal β7α7β8α8 unit to the rest of the protein (Fig. 1). Also, it has been previously shown that this salt bridge is an important mediator of a hydrogen bonding network imperative for the catalytic capacity and stability of TPI (5). Mutations at this salt bridge could impair human TPI dimer stability, or lead to TPI aggregation.

To examine how R189 mutations influence the physical and biochemical properties of TPI, we purified human TPI^{WT}, TPI^{R189A}, and TPI^{R189Q}. TPI purification was performed as outlined previously [20], and although successful, the R189 mutants yielded far less enzyme compared to TPI^{WT}. The migration of these enzymes through native gel electrophoresis was used as a primary strategy to assess quaternary structure. In this assay, any aggregated protein would not be able to

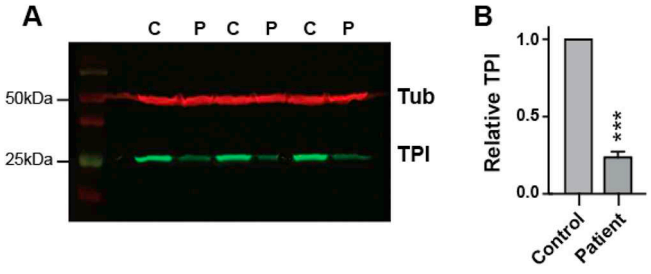

Fig. 5. Total TPI protein levels are reduced in fibroblasts from TPI^{E104D}/TPI^{R189Q} patient. A) A representative western blot probing fibroblast samples from the TPI deficient proband (P) and a healthy patient as a control (C). Beta-tubulin (Tub) was used as a loading control in the experiment. B) Quantification of relative TPI signal reveal a significant reduction in total TPI protein levels in the proband compared to control. Differences were evaluated with Student's *t*-test, *** p value < 0.0001, n = 3.

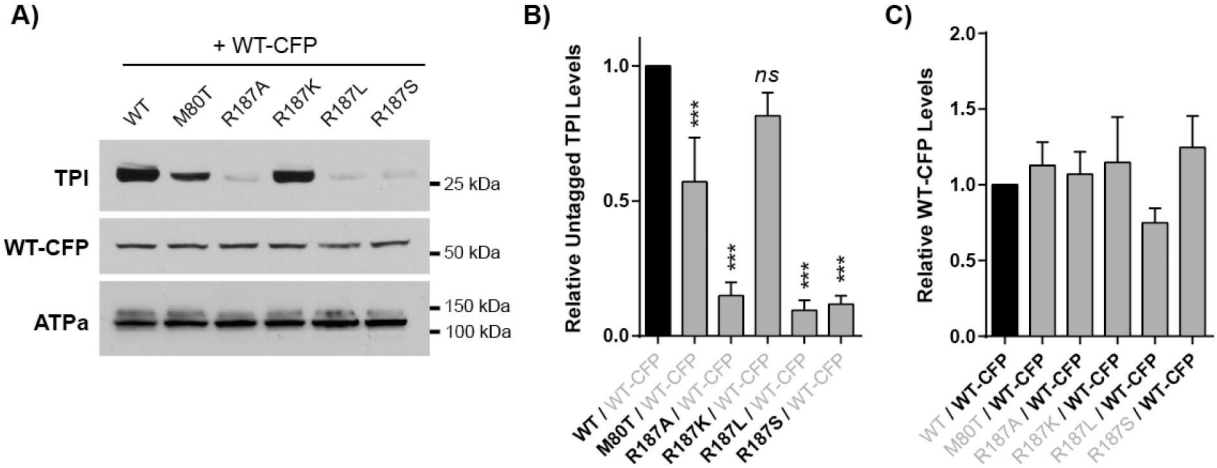

Fig. 4. Mutations that alter the basic chemistry of TPI^{R187} reduce protein levels in vivo. Animals heterozygous for a CFP-tagged wild type TPI were generated, lysates collected, and probed via western blot. A) A representative image of a western blot probed for anti-TPI or anti-ATPα. ATPα was used as a loading control. Untagged TPI variants migrated at ~27 kDa, and the CFP-tagged version at ~54 kDa. B) and C) are quantifications of the densities of untagged (~27 kDa) and CFP-tagged (~54 kDa) bands, respectively. Quantification was made using density measurements of bands produced from three independent replicates (n = 3, ± S.D.). Variance was assessed with a one-way ANOVA, and comparisons to WT were made using Tukey's post hoc test. *** indicates $p < 0.001$, while *ns* indicates no significance.

Table 1
R189 substitutions alter protein stability but not dimerization.

Sample	Radius (nm)	Melting temperature (°C)
Wild type	3.5 ± 0.1	49.8 ± 0.4
R189A	3.8 ± 0.1	62.1 ± 0.8
R189Q	4.0 ± 0.2	59.2 ± 0.7

Table 2
Data collection and refinement statistics.

PDB ID: 6NLH	Human TPI R189A
Data collection	
Space group	P1
Cell dimensions	
a, *b*, *c* (Å)	65.142 73.661 92.842
α, β, γ (°)	90.031 90.026 89.999
Unique reflections	84,091
Resolution (Å)	50.0–2.20 (2.24–2.20)[a]
R_{merge} (%)[b]	8.1 (41.4)
$I / \sigma I$	16.8 (3.29)
Completeness (%)	96.0 (93.8)
Redundancy	2.5
Refinement	
Resolution (Å)	20.0–2.20
R_{work}[c] / R_{free}[d] (%)	17.8/21.4
Number of non-hydrogen atoms	
Protein	15,388
Solvent and ligands	818
B-factors (Å^2)	
Protein	35.0
Solvent	29.5
R.m.s. deviations	
Bond lengths (Å)	0.006
Bond angles (°)	0.67
Ramachandrian	
Outliers (%)	0.0
Allowed (%)	2.6
Favored (%)	97.4
Clashscore	3.15

[a] Values in parentheses are for highest-resolution shell.
[b] $R_{merge} = (|(\Sigma I - < I >)|)/(\Sigma I)$, where $< I >$ is the average intensity of multiple measurements.
[c] $R_{work} = \Sigma_{hkl}||F_{obs}(hkl)|| - F_{calc}(hkl)||/\Sigma_{hkl}|F_{obs}(hkl)|$.
[d] R_{free} represents the cross-validation *R* factor for 1.5% (~1250) of the reflections against which the model was not refined.

migrate into the gel and would be retained at the top, or changes in protein homogeneity could be observed as differences in the coherence of the observed band. We observe that both R189A and R189Q mutants have a slightly higher mobility compared to WT, consistent with the loss of a charged residue (Fig. S1). In all cases, no protein was detected in the well or in the stacking layer of the gel, leading us to conclude that the R189A and R189Q mutants do not cause significant protein aggregation in vitro. To evaluate whether these mutations may influence dimerization, we measured the hydrodynamic radius of all enzyme variants using dynamic light scattering (DLS). DLS measurements revealed that the two mutations of R189 do not reduce the hydrodynamic radius of the enzyme, suggesting that the dimer is intact (Table 1). Conversely, the radius is slightly larger for both mutants (Table 1), suggesting that the enzyme in solution may be more flexible than the WT variant (See Table 2.)

We next tested the stability of these proteins using differential scanning fluorimetry. In this assay, the fluorescence of a hydrophobic dye increases as it interacts with non-polar residues of a protein that are exposed during thermal denaturation. Thermal denaturation revealed that both R189A and R189Q mutants exhibit single-phase, non-reversible denaturation (Fig. S2). WT TPI exhibits a T_m of 49.8 ± 0.4 °C, while both mutations of R189 shifted the melting temperature to 62.1 ± 0.8 °C and 59.2 ± 0.7 °C for the R189A and R189Q, respectively (Table 1). These data suggest that all three TPI enzymes are stably folded, and that the folded R189 mutants require more energy to intrinsically denature.

Structural studies indicate abnormal coordination of catalytic residues proximal to R189.

In an effort to understand the effect that mutations at the R189 position might have on the structure of TPI, we have purified, crystallized, and determined the structure of TPI^{R189A} at 2.2 Å resolution. Crystals were obtained in conditions similar to wild-type [20] in an effort to minimize the impact the crystallization environment might play on changes induced by the mutant. Despite this, the morphology of the crystals were different, and produced rod-like crystals which belong to space group P1, and contained 8 copies of TPI^{R189A} in the asymmetric unit, arranged into 4 TPI dimers. Wild-Type TPI buries 1705 Å^2 at its dimer interface, while TPI^{R189A} buries between 1692 and 1728 Å^2 with its 4 dimers; therefore, the structure indicates that the R189A mutant protein is also a dimer. Overall, the fold of each TPI^{R189A} was nearly identical to the previously reported TPI^{WT} (r.m.s.d = 0.13–0.27 for the eight TPI^{R189A} chains in the structure). In the vicinity of amino acid 189, we find that the side chains for residues D225 and D227 are both repositioned very slightly, partially filling in the void left by the absent arginine side chain (Fig. 6A).

In wild-type TPI structures both from our group and others [14,15,20,33–36], the formation of a catalytically competent active site is controlled by movements of a lid formed by residues 165–175, which has been observed in both open and closed conformations. Under these crystallization conditions, the closed conformation is associated with the presence of an ordered phosphate and bromide ion, which occupy positions taken by phosphate and triose moieties in the TPI substrate co-complex [20]. Only one monomer in the TPI dimer adopts this closed conformation in the 4POC wild-type structure [20]. Motions of the lid are controlled by movements at the N-hinge and C-hinge regions (residues 165–167, and 173–175 respectively) [15,37]. Movement of the lid into the closed position, associated with a substrate bound state, results in E165 being shifted into a catalytically competent position. Interestingly, we find numerous differences between TPI^{WT} and TPI^{R189A} in the catalytic lid region. First, we find the positioning of the E165 side chain is in the catalytically inactive position in all 8 monomers within the asymmetric unit (Fig. 6B). This is true regardless of the presence of phosphate and bromide ions which are found in 4 monomers. Thus, despite containing interactions which mimic the substrate bound state, TPI^{R189A} does not reposition E165. Second, in active sites that contain phosphate and bromide ions, the lid was not ordered, indicating that its position was flexible and not being held into the closed state (Fig. 6B). The positioning of N-hinge residues 166–168 are significantly different than the occupied wild-type, consistent with those residues being tucked into the core of the protein (Fig. 6C). The internal orientation of residues 166–168 is observed within the “inactive” monomer of the TPI^{WT} dimer with the lid open (Fig. 6C); however, in TPI^{R189A} the catalytic lid is disordered. The movement of the conserved W168 of the N-hinge is known to be critical to the integrity of loop6 [38]. The nitrogen of the indole ring hydrogen bonds to the carboxyl of E129 in the closed state, and swaps to the hydroxyl of Y164 in the open conformation (Fig. S3). These three residues are constitutively bonded, but the organization of the bonding changes as the lid closes and W168 moves away from Y164 (Figs. 6C, S3). The alternating coupling of Y164::W168 and E129::W168 are thought to be a part of how the conserved P166 fulcrums E165 toward the “swung in” and “swung out” positions [15,37,39]. In the TPI^{R189A} structure, W168 does not alter its organization within this network regardless of catalytic site occupancy (Figs. 6C, S3). Finally, the occupied state of loop6 has also been shown to be stabilized by the loop-clamping side chains Y208 and S211 of loop7 (Fig. 6D) [40]. The hydroxyl of Y208 hydrogen bonds with the amide backbone of A176 in the occupied state, while the hydroxyl of S211 establishes two hydrogen bonds to the peptide backbone of A169 and G173 [40]. Further, the closure of loop6 helps to position the amide

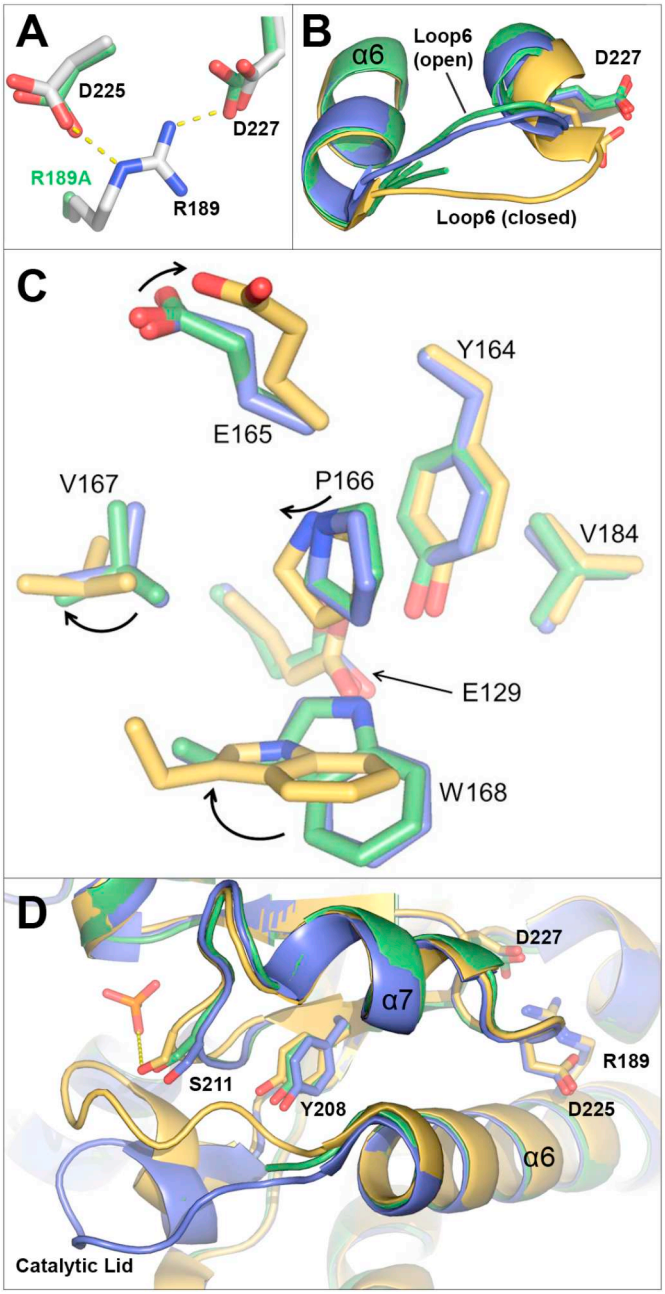

Fig. 6. TPI^{R189A} breaks a conserved salt bridge in helix 6 and consequently influences loop6 open and close conformations. A) The R189 salt bridge in wild-type (white) and R189A mutant (green). Wild-type enzyme mediates two hydrogen bonding interactions with D225 and D227 via R189. There is not a significant repositioning of the D225/227 loop in response to the R189A alteration, just a slight rearrangement in the positioning of these side chains. B) The TPI catalytic lid. Wild-type TPI dimer contains one lid in the catalytically competent position (yellow, closed) and one in the incompetent, open position (blue). All 8 monomers of R189A are either in the open position or are disordered (only 3 of the R189A monomers are shown her for clarity, in green), with the catalytic E165 residue in the "swung out" orientation. C) The N-hinge. Residues coloured as in (B) without backbone for positional clarity. Arrows indicate residue movements from 'open' to 'closed' positions within the wild-type enzyme. D) The loop7. Cartoon is coloured as in (B), with loop7 residues Y208 and S211 shown in sticks. A hydrogen bond to the phosphate ion is dashed, with the phosphate ion shown in sticks. (For interpretation of the references to colour in this figure legend, the reader is referred to the web version of this article.)

backbone of S211 into a position where it hydrogen bonds with the active site phosphate [41]. Interestingly, we find that the loop7 residues in TPI^{R189A} are positioned halfway between the "open" and "closed" conformations, with the amide backbone of S211 more closely aligning with the closed conformation, while the side-chain hydroxyl protrudes toward where the loop6 in a way similar to occupied TPI^{WT} (Fig. 6D). Collectively, these observations support the conclusion that the TPI^{R189A} active site is still competent to bind substrate (as mimicked through phosphate and bromide ions); however, it does not adopt a conformation consistent with a closed catalytically competent enzyme.

3. Discussion

We report here evidence of a new pathogenic allele associated with TPI deficiency. The proband of this study is a compound heterozygote carrying *TPI*^{E104D} and *TPI*^{R189Q} alleles. *TPI*^{E104D} is one of six known TPI deficiency mutations, and the most common disease-associated allele. However, mutations in *TPI*^{R189} had not previously been associated with the disease. The patient exhibited increased susceptibility to infections, neurologic impairment, and anemia; hallmarks of the disease. To determine whether *TPI*^{R189} mutations could themselves be pathogenic, we mutated this conserved R189 in *Drosophila*. The homologous arginine in *Drosophila* is at position 187 (Fig. 3A), and mutations that altered the basic chemistry of *Drosophila TPI*^{R187} elicited homozygous lethality. Conversely, a functionally conserved substitution, *TPI*^{R187K}, was homozygous viable and behaviourally normal. Finally, we demonstrated that *TPI*^{R187} mutations could exacerbate the neurologic deficits caused by the *TPI*^{M80T} mutation in compound heterozygote animals. These findings suggest that *TPI*^{R189Q} elicits a strong loss-of-function that can elicit neurologic disease in compound heterozygote patients.

Mutating the conserved R189 reduces protein levels in patient fibroblasts and *Drosophila* animal models. Mutations that alter the folding or stability of a protein can lead to reduced protein levels in vivo, leading us to purify and examine the protein. Previous TPI structural studies have highlighted the presence of the solvent-exposed salt bridge formed by R189 and D225/D227 [42,43]. This bridge links helix 6 and helix 7 on the side of the TIM barrel opposite of the dimer interface. Mutational analysis of this conserved arginine in *Trypanosoma* revealed that it was an important determinant of protein stability [22]. Further, altering the acidic chemistry of D225 in yeast impaired TPI folding [43]. Our findings here suggest that the patient mutation is likely impacting both folding and stability, culminating in reduced protein levels. We purified human TPI^{R189A} and TPI^{R189Q} proteins, and gel electrophoresis (Fig. S1) and DLS confirmed that these R189 mutants were forming dimers. Yet the hydrodynamic radius of the R189 mutants suggested that these enzymes were more flexible than WT (Table 1). The crystal structure of TPI^{R189A} demonstrates that the enzyme improperly folds the catalytic lid, loop6 (Fig. 6), and the disordered character of this loop could explain its increased hydrodynamic radius. Interestingly, thermal denaturing experiments using a hydrophobic fluorescent dye suggest that the R189 mutants were more resistant than WT to thermal denaturation (Table 1, Fig. S2). These results are the opposite of what was reported in the *Trypanosomal* protein using circular dichroism, and may be attributable to differences between the enzymes or methodologies.

The catalytic lid of human TPI is influenced by R189. We purified, crystallized, and determined the structure of TPI^{R189A} to examine how this mutation could physically alter the biochemistry of this enzyme. Unexpectedly, the primary difference in the wild type and R189A structures was the organization of the catalytic site; specifically i) the catalytic lid (loop6), ii) the catalytic E165, iii) the N-hinge, and iv) the loop6-clamping residues of loop7. These four structures are mechanistically linked: the N-hinge immediately proceeds the catalytic E165, and the orientation of this acidic residue is in part influenced by its neighbouring P166. The peptide backbone in this region is thought to be torqued by the movement of the conserved W168 (Fig. 6C). The

indole ring of W168 hydrogen bonds with two nearby residues, Y164 and E129 (Fig. S3). The organization of this hydrogen bonding triad is necessary for catalysis, and the activity of the enzyme is reduced as the movement of the catalytic lid is impaired [15,17]. Indeed, a *W168F* substitution at the N-hinge has been shown to disorder the lid [38].

It is currently unclear how the R189A mutation physically influences the organization of the N-hinge. One hypothesis is that the movement of the N-hinge may be influenced by helix 6 through V184, which buttresses Y164 through van der Waals interactions (Fig. 6C). V184 is one helix turn from R189, therefore changes to this basic residue could be predicted to break the salt bridge necessary for maintaining the integrity of helix 6, and thereby supporting the movements of the catalytic lid. However, we do not see any changes in the density of V184 in the TPI^{R189A} structure, therefore our current data cannot rigorously test this hypothesis. It is possible that the confines of the crystal lattice may be preventing additional motions in the V184 region. A second possibility is that the R189::D225/D227 salt bridge is important for positioning the backbone of the loop7 residues Y208 and S211. Loop7 helps to stabilize the "closed" or occupied state of the catalytic site through hydrogen bonds formed with the backbone of the catalytic lid as well as the substrate. Residues Y208 and S211 are seen in an intermediate conformation in the TPI^{R189A} structure, relative to the positions taken when in the "open" and "closed" WT enzyme. The inability for these residues to fully shift and clamp the catalytic lid in the occupied state may contribute to the instability of loop6 in the TPI^{R189A} mutant.

The rigid flexibility of TPI's catalytic lid (loop6) is a key physical mechanism for directing the isomerization of DHAP [36]. The closure of this enzyme lid limits the access of water molecules to the substrate intermediate [44]. As the proton of DHAP is being shuttled by E165, the former carbonyl backbone of the enediol phosphate intermediate is exceedingly sensitive to attack by water [36,45,46]. In solution, this reaction readily forms the toxic by-product, methylglyoxal [47]. However, TPI facilitates the selective isomerization of its substrate by protecting these reaction intermediates and stabilizing the charged transition state in the conversion of DHAP to G3P [48]. A previous study has even gone so far as to purposefully create an artificial methylglyoxal synthase by simply deleting the loop6 lid of the TPI enzyme, thus stabilizing the substrate intermediates without protecting them from solvent [36]. The disordered nature of this catalytic lid could thus potentially trigger recognition by quality control mechanisms within the cell. The TPI^{M80T} (a.k.a. $TPI^{sugarkill}$) mutation in *Drosophila* is known to be recognized by Hsp70 and Hsp90, and then targeted to the proteasome for degradation and genetic or pharmacologic impairment of HsP70/90 or the proteasome improves longevity, demonstrating that mutant TPI retains function and increased turnover is a critical part of disease pathogenesis [21]. Therefore, protein misfolding, recognition, and proteasome degradation could explain why TPI^{R189} mutations lead to reduced protein levels in humans and flies, without substantially reducing thermostability in vitro. Furthermore, since TPI is an essential enzyme in organisms from *E coli* to humans, it is reasonable to propose that one common class of disease-causing *TPI* mutations may retain TPI catalytic function but have reduced steady-state levels due to increased turnover of the mutant protein.

We propose that mitigating mutant TPI degradation may be an effective therapy for several, if not most, pathogenic TPI deficiency mutations. There are no current therapies for treating the neurological symptoms of TPI deficient patients. Bone marrow transplants have been tested in mice [49] and humans (personal communication), and an animal study found that it corrected red blood cell defects in a murine model of TPI deficiency [49]. These results are promising for the hematologic components of the disease, but a recent study has suggested that the neurologic dysfunction associated with TPI deficiency is intrinsic to vesicle recycling defects in neurons [29]. These observations suggest that an effective neurologic therapy may need to target the peripheral or central nervous system. In an animal model of TPI deficiency, proteasome inhibitors were systemically administered and shown to attenuate behavioural dysfunction in a *Drosophila* model of TPI deficiency [21]. The proteasome inhibition was shown to support levels of the dimer mutant, TPI^{M80T}, which is prone to protein degradation. We have reported here that TPI^{E104D}/TPI^{R189Q} patient fibroblasts have approximately 25% the normal levels of TPI enzyme (Fig. 5). Therefore, proteasome inhibitors may provide a new therapeutic avenue for treating neurologic dysfunction in TPI deficiency. Indeed, several proteasome inhibitors have already obtained FDA approval for oncology indications. First and second-generation proteasome inhibitors have been used to treat multiple myeloma and mantle-cell lymphoma, with side-effects including peripheral neuropathy [50–52]. Although these secondary responses may seem counterproductive for treating neurologic disease, they indicate that these drugs are having an impact on the nervous system and may require alternative administration or dosing. Pre-clinical and clinical studies will be needed to more thoroughly evaluate the therapeutic potential of these compounds in TPI deficiency.

In conclusion, the data presented in this study highlights a new pathogenic mutation that contributes to TPI deficiency in patients. Mutations affecting the R189 residue in humans or in flies (TPI^{R187}) causes reduced TPI enzyme levels, and this may be structurally induced by changes in the folding of the enzyme lid. These results are critical for directing future pre-clinical and clinical studies aimed at developing therapeutic strategies for attenuating the neurologic dysfunction seen in TPI deficient patients.

4. Materials and methods

4.1. Haematological and enzyme assays

Blood samples from patient and parents were collected after obtaining informed consent. Routine haematological investigations were carried out according to [53]. TPI activity was determined according to [54]. All the diagnostic procedures and investigations were performed in accordance with the Helsinki Declaration of 1975.

4.2. Molecular analysis of TPI gene

Genomic DNA was extracted from leucocytes using standard manual methods. The entire codifying region and intronic flanking regions of *TPI1* gene were analyzed by direct sequencing (ABI PRISM 310 Genetic Analyzer; Applied Biosystems, Warrington, UK) using Big Dye Terminator Cycle Sequencing kit (Applied Biosystems). Nucleotide numbering refers to NCBI Reference Sequence NM_000365.5. TPI sequences used for alignments were Hs_TPI (CAA49379.1), Dm_TPI (CAA40804.1), Mm_TPI (CAA37420.1), Gg_TPI (NP_990782.1), Sc_TPI (ONH79887.1), Tb_TPI (CAA27559.1), and Ec_TPI (ADX52952.1). Details about the R189Q variant have been deposited in NCBI's ClinVar database (SCV000882820).

4.3. Patient fibroblasts

Patient cells were obtained from a 4-year-old female TPI deficiency patient via skin punch using University of Pittsburgh approved IRB 0404017. Cells were cultured using standard methods (37C, 5% CO_2) in complete media (DMEM with 10% serum, 100u penicillin/100 μg streptomycin/ml (Lonza), 2 mM L-glutamine (Gibco) and supplemental non-essential amino acids (Gibco). The cells were de-identified and are known only as FB887.

4.4. Drosophila husbandry and strains

Drosophila strains were maintained on standard cornmeal molasses media at room temperature in a 12:12 light:dark cycle, unless indicated.

4.5. Mutagenesis and genomic engineering

Site directed mutagenesis was achieved using the QuikChange Lightening Site-Directed Mutagenesis Kit (Agilent Technologies). Oligomeric mutagenic primers were engineered (Integrated DNA technologies) to introduce an arginine-to-alanine/lysine/leucine/serine change at position 187 (TPI^{R187A}, TPI^{R187K}, TPI^{R187L}, TPI^{R187S}). Mutations were generated on the *pGE-attBTPI*$^{+}$ plasmid and confirmed via sequencing [28]. Once generated, the constructs were injected into the embryos generated by mating of; *PGX-TPI* founder line males crossed with *vasa-phiC31*$^{ZH\text{-}2A}$; virgin females for in genomic engineering [55]. F1 progeny were screened for integration indicated by w^{+} expression, and integration was confirmed by sequencing.

4.6. Drosophila behavioural testing

Approximately equivalent numbers of males and females were collected and aged 3 days at 25 °C on standard molasses-based media. At testing, mechanical stress sensitivity was determined by vortexing flies in a standard vial for 20 s and measuring their subsequent time to recovery [56]. Recovery was scored following two purposeful movements, such as righting, grooming, or walking, and behavioural responses were capped at 360 s. A one-way ANOVA assessed variance in the behavioural responses, and Tukey's post hoc test was used to compare genotypes.

4.7. Western blotting

Drosophila immunoblotting was performed as outlined previously [29]. Blots were incubated with anti-TPI (1:5000; rabbit polyclonal FL-249; Santa Cruz Biotechnology) or anti-ATPalpha (1:10,000; mouse monoclonal alpha5; Developmental Studies Hybridoma Bank). Densitometric analyses of the scanned films were performed on unsaturated exposures using ImageJ software available from the National Institutes of Health. A one-way ANOVA was performed to assess variance of TPI levels and data sets were compared using Tukey's post-hoc analysis.

Human fibroblasts were trypsinized (0.05% for 5 min), pelleted, resuspended in RIPA buffer with protease inhibitors (PMSF (100uM), Leupeptin (1 μg/uL), Pepstatin A (0.5 μg/uL)) and were pulse sonicated. Protein concentrations were determined using a BCA assay (Pierce). Immunoblotting was performed on whole protein cell lysates following the addition of an equal volume of 2× SDS PAGE sample buffer (4% SDS, 4% β-mercaptoethanol, 130 mM Tris HCl pH 6.8, 20% glycerol). Proteins were resolved by SDS-PAGE (12%), transferred onto 0.45 μm PVDF membrane. The blots were blocked in Odyssey Blocking Buffer (Licor) and incubated with anti-TPI (1:5000; rabbit polyclonal FL-249; Santa Cruz Biotechnology) or anti-Beta-tubulin (1:1000; mouse polyclonal E7-C; Developmental Studies Hybridoma Bank) diluted in Odyssey Blocking Buffer (Licor). Following washes in PBST, the blots were incubated with anti-mouse-IR800 (Fisher Scientific) and anti-rabbit-IR680 (Molecular Probes) both diluted to 1:20,000 in 0.1% Tween 20 blocking buffer. Blots were washed in PBST and developed using Odyssey Infrared Imaging System. Quantification of the scanned films was performed digitally using ImageJ software available from the National Institutes of Health. Differences of TPI levels were evaluated by a two-tailed Student's *t*-test.

4.8. TPI protein purification

Wild-type and mutant TPI proteins were expressed in E.coli, BL21 (DE3) Codon+ cells using ZY autoinduction media [57]. Cell were collected by centrifugation and lysed via homogenization in a buffer containing 25 mM Tris pH 8.0, 500 mM NaCl, 10% glycerol, 5 mM imidazole, and 1 mM β-mercaptoethanol. The lysate was cleared by centrifugation, and TPI was purified by nickel affinity chromatography. Overnight digestion using TEV protease followed by a second round of Nickel affinity chromatography was used to remove the His_6-MBP tag and other contaminants. Anion exchange chromatography and gel filtration chromatography were performed as final polishing steps. Peak fractions of TPI^{R189A} from gel filtration that were used for crystallization were dialyzed into 20 mM Tris pH 8.8, 25 mM NaCl, 2.0% glycerol, and 1 mM β-mercaptoethanol and concentrated to 4.55 mg/mL.

4.9. Crystallization and structure determination

TPI^{R189A} crystals were obtained using the sitting drop vapor diffusion method at 4 °C. Crystals grew within 2 days in a drop containing 1 μL of protein and 2 μL of the 28% PEG 2000, 50 mM KBr reservoir solution. Crystals were cryoprotected in 40% PEG 2000, 10% glycerol, and 50 mM KBr and flash frozen in liquid nitrogen prior to x-ray diffraction. Diffraction data was collected at our home source using a Rigaku FR-E generator and RAXIS4-HTC detector. Diffraction data were integrated, scaled, and merged using HKL2000 [58] using an $I/\sigma I$ cutoff of 2.0. $hTPI^{R189A}$ crystals belong to the space group P1 (a = 65.142 Å, b = 73.661 Å, c = 92.842 Å; β = 90.026°) and contain 4 dimers in the asymmetric unit. Initial phases were estimated via molecular replacement using a search model derived from an independent structure of human TPI (2JK2) [19]. The model was then refined and improved by manual rebuilding within Coot [59] combined with simulated annealing, positional, and isotropic B factor refinement within Phenix. Model quality was assessed using MolProbity [60]. Structural figures were generated using PyMol (PyMOL Molecular Graphics System, Version 1.5.0.4, Schrödinger, LLC.). The coordinates and structure factors associated with $hTPI^{R189A}$ structures have been deposited within the Protein Databank under accession code 6NLH.

4.10. Thermal shift assays

The thermal stability of $hTPI^{R189A}$ and $hTPI^{R189Q}$ mutants relative to wild type were determined using a protein thermal shift assay [61]. Proteins assayed were diluted to 0.1 mg/mL in a buffer containing 15 mM Tris pH 8.8, 200 mM NaCl, 5% glycerol, 1 mM β-mercaptoethanol, and 1.7× SYPRO Orange. Fluorescence of SYPRO Orange was measured and plotted as a function of temperature to quantify protein unfolding. The T_m was defined as the temperature with the maximum rate of change in fluorescence.

4.11. Dynamic light scattering

TPI^{R189A}, TPI^{R189Q}, and wild type proteins were diluted to a final concentration of 0.5 mg/mL in a buffer containing 15 mM Tris pH 8.8, 200 mM NaCl, 5% glycerol, and 1 mM β-mercaptoethanol. Dynamic light scattering measurements were taken on a DynaPro NanoStar and analyzed using the DYNAMICS software package.

Transparency document

The Transparency document associated this article can be found, in online version.

Acknowledgements

We are grateful for the support of our Departments (Pharmacology & Chemical Biology, Biological Sciences and Pediatrics) and the Pittsburgh Institute for Neurodegenerative Diseases (PIND) at the University of Pittsburgh. We also are grateful for financial support from the Achievement Rewards for College Scientists Foundation: Pittsburgh Chapter, and National Institutes of Health (NIH) grants R21AG059385, R21NS095614, R01GM108073, R21AG059386, and T32GM8424-17.

Appendix A. Supplementary data

Supplementary data to this article can be found online at https://doi.org/10.1016/j.dummy.2019.01.002.

References

[1] F. Orosz, J. Olah, J. Ovadi, Triosephosphate isomerase deficiency: new insights into an enigmatic disease, Biochim. Biophys. Acta 1792 (2009) 1168–1174.
[2] N. Sarper, E. Zengin, C. Jakobs, G.S. Salomons, M. Mc Wamelink, M. Ralser, K. Kurt, B. Kara, Mild hemolytic anemia, progressive neuromotor retardation and fatal outcome: a disorder of glycolysis, triose- phosphate isomerase deficiency, Turk. J. Pediatr. 55 (2013) 198–202.
[3] R.E. Linarello, A.K. Shetty, T. Thomas, R.P. Warrier, Triosephosphate isomerase deficiency in a child with congenital hemolytic anemia and severe hypotonia, Pediatr. Hematol. Oncol. 15 (1998) 553–556.
[4] S.W. Eber, A. Pekrun, A. Bardosi, M. Gahr, W.K. Krietsch, J. Kruger, R. Matthei, W. Schroter, Triosephosphate isomerase deficiency: haemolytic anaemia, myopathy with altered mitochondria and mental retardation due to a new variant with accelerated enzyme catabolism and diminished specific activity, Eur. J. Pediatr. 150 (1991) 761–766.
[5] R. Rosa, M.O. Prehu, M.C. Calvin, J. Badoual, D. Alix, R. Girod, Hereditary triose phosphate isomerase deficiency: seven new homozygous cases, Hum. Genet. 71 (1985) 235–240.
[6] L. Manco, M.L. Ribeiro, Novel human pathological mutations. Gene symbol: TPI1. Disease: triosephosphate isomerase deficiency, Hum. Genet. 121 (2007) 650.
[7] J.M. Wilmshurst, G.A. Wise, J.D. Pollard, R.A. Ouvrier, Chronic axonal neuropathy with triosephosphate isomerase deficiency, Pediatr. Neurol. 30 (2004) 146–148.
[8] R. Arya, M.R. Lalloz, A.J. Bellingham, D.M. Layton, Evidence for founder effect of the Glu104Asp substitution and identification of new mutations in triosephosphate isomerase deficiency, Hum. Mutat. 10 (1997) 290–294.
[9] G. Serdaroglu, Y. Aydinok, S. Yilmaz, L. Manco, E. Ozer, Triosephosphate isomerase deficiency: a patient with Val231Met mutation, Pediatr. Neurol. 44 (2011) 139–142.
[10] M.L. Chang, P.J. Artymiuk, X. Wu, S. Hollan, A. Lammi, L.E. Maquat, Human triosephosphate isomerase deficiency resulting from mutation of Phe-240, Am. J. Hum. Genet. 52 (1993) 1260–1269.
[11] S. Hollan, H. Fujii, A. Hirono, K. Hirono, H. Karro, S. Miwa, V. Harsanyi, E. Gyodi, M. Inselt-Kovacs, Hereditary triosephosphate isomerase (TPI) deficiency: two severely affected brothers one with and one without neurological symptoms, Hum. Genet. 92 (1993) 486–490.
[12] W. Schliebs, N. Thanki, R. Jaenicke, R.K. Wierenga, A double mutation at the tip of the dimer interface loop of triosephosphate isomerase generates active monomers with reduced stability, Biochemistry 36 (1997) 9655–9662.
[13] R.K. Wierenga, E.G. Kapetaniou, R. Venkatesan, Triosephosphate isomerase: a highly evolved biocatalyst, Cell. Mol. Life Sci. 67 (2010) 3961–3982.
[14] V. Pareek, M. Samanta, N.V. Joshi, H. Balaram, M.R. Murthy, P. Balaram, Connecting active-site loop conformations and catalysis in triosephosphate isomerase: insights from a rare variation at residue 96 in the plasmodial enzyme, Chembiochem 17 (2016) 620–629.
[15] J. Xiang, J. Sun, N.S. Sampson, The importance of hinge sequence for loop function and catalytic activity in the reaction catalyzed by triosephosphate isomerase, J. Mol. Biol. 307 (2001) 1103–1112.
[16] N.S. Sampson, J.R. Knowles, Segmental motion in catalysis: investigation of a hydrogen bond critical for loop closure in the reaction of triosephosphate isomerase, Biochemistry 31 (1992) 8488–8494.
[17] J. Sun, N.S. Sampson, Understanding protein lids: kinetic analysis of active hinge mutants in triosephosphate isomerase, Biochemistry 38 (1999) 11474–11481.
[18] N. Cabrera, A. Torres-Larios, I. Garcia-Torres, S. Enriquez-Flores, R. Perez-Montfort, Differential effects on enzyme stability and kinetic parameters of mutants related to human triosephosphate isomerase deficiency, Biochim. Biophys. Acta Gen. Subj. 1862 (2018) 1401–1409.
[19] C. Rodriguez-Almazan, R. Arreola, D. Rodriguez-Larrea, B. Aguirre-Lopez, M.T. de Gomez-Puyou, R. Perez-Montfort, M. Costas, A. Gomez-Puyou, A. Torres-Larios, Structural basis of human triosephosphate isomerase deficiency: mutation E104D is related to alterations of a conserved water network at the dimer interface, J. Biol. Chem. 283 (2008) 23254–23263.
[20] B.P. Roland, C.G. Amrich, C.J. Kammerer, K.A. Stuchul, S.B. Larsen, S. Rode, A.A. Aslam, A. Heroux, R. Wetzel, A.P. VanDemark, M.J. Palladino, Triosephosphate isomerase I170V alters catalytic site, enhances stability and induces pathology in a Drosophila model of TPI deficiency, Biochim. Biophys. Acta 1852 (2015) 61–69.
[21] S.L. Hrizo, M.J. Palladino, Hsp70- and Hsp90-mediated proteasomal degradation underlies TPI sugarkill pathogenesis in Drosophila, Neurobiol. Dis. 40 (2010) 676–683.
[22] I. Kursula, S. Partanen, A.M. Lambeir, R.K. Wierenga, The importance of the conserved Arg191-Asp227 salt bridge of triosephosphate isomerase for folding, stability, and catalysis, FEBS Lett. 518 (2002) 39–42.
[23] S.H. Orkin, D.G. Nathan, Nathan and Oski's Hematology of Infancy and Childhood, 7th ed., Saunders/Elsevier, Philadelphia, 2009.
[24] F. Orosz, J. Olah, J. Ovadi, Triosephosphate isomerase deficiency: facts and doubts, IUBMB Life 58 (2006) 703–715.
[25] C. Valentin, S. Pissard, J. Martin, D. Heron, P. Labrune, M.O. Livet, M. Mayer, T. Gelbart, A. Schneider, I. Max-Audit, M. Cohen-Solal, Triose phosphate isomerase deficiency in 3 French families: two novel null alleles, a frameshift mutation (TPI Alfortville) and an alteration in the initiation codon, TPI Paris, Blood 96 (2000) 1130–1135.
[26] J. Bendl, J. Stourac, O. Salanda, A. Pavelka, E.D. Wieben, J. Zendulka, J. Brezovsky, J. Damborsky, PredictSNP: robust and accurate consensus classifier for prediction of disease-related mutations, PLoS Comput. Biol. 10 (2014) e1003440.
[27] K.A. Jagadeesh, A.M. Wenger, M.J. Berger, H. Guturu, P.D. Stenson, D.N. Cooper, J.A. Bernstein, G. Bejerano, M-CAP eliminates a majority of variants of uncertain significance in clinical exomes at high sensitivity, Nat. Genet. 48 (2016) 1581–1586.
[28] B.P. Roland, K.A. Stuchul, S.B. Larsen, C.G. Amrich, A.P. Vandemark, A.M. Celotto, M.J. Palladino, Evidence of a triosephosphate isomerase non-catalytic function crucial to behavior and longevity, J. Cell Sci. 126 (2013) 3151–3158.
[29] B.P. Roland, A.M. Zeccola, S.B. Larsen, C.G. Amrich, A.D. Talsma, K.A. Stuchul, A. Heroux, E.S. Levitan, A.P. VanDemark, M.J. Palladino, Structural and genetic studies demonstrate neurologic dysfunction in triosephosphate isomerase deficiency is associated with impaired synaptic vesicle dynamics, PLoS Genet. 12 (2016) e1005941.
[30] A.M. Celotto, A.C. Frank, J.L. Seigle, M.J. Palladino, Drosophila model of human inherited triosephosphate isomerase deficiency glycolytic enzymopathy, Genetics 174 (2006) 1237–1246.
[31] J.P. Gnerer, R.A. Kreber, B. Ganetzky, Wasted away, a drosophila mutation in triosephosphate isomerase, causes paralysis, neurodegeneration, and early death, Proc. Natl. Acad. Sci. U. S. A. 103 (2006) 14987–14993.
[32] J.L. Seigle, A.M. Celotto, M.J. Palladino, Degradation of functional triose phosphate isomerase protein underlies sugarkill pathology, Genetics 179 (2008) 855–862.
[33] Q. Liao, Y. Kulkarni, U. Sengupta, D. Petrovic, A.J. Mulholland, M.W. van der Kamp, B. Strodel, S.C.L. Kamerlin, Loop motion in triosephosphate isomerase is not a simple open and shut case, J. Am. Chem. Soc. 140 (2018) 15889–15903.
[34] Z. Zhang, S. Sugio, E.A. Komives, K.D. Liu, J.R. Knowles, G.A. Petsko, D. Ringe, Crystal structure of recombinant chicken triosephosphate isomerase-phosphoglycolohydroxamate complex at 1.8-a resolution, Biochemistry 33 (1994) 2830–2837.
[35] K.U. Yuksel, A.Q. Sun, R.W. Gracy, K.D. Schnackerz, The hinged lid of yeast triosephosphate isomerase. Determination of the energy barrier between the two conformations, J. Biol. Chem. 269 (1994) 5005–5008.
[36] D.L. Pompliano, A. Peyman, J.R. Knowles, Stabilization of a reaction intermediate as a catalytic device: definition of the functional role of the flexible loop in triosephosphate isomerase, Biochemistry 29 (1990) 3186–3194.
[37] I. Kursula, M. Salin, J. Sun, B.V. Norledge, A.M. Haapalainen, N.S. Sampson, R.K. Wierenga, Understanding protein lids: structural analysis of active hinge mutants in triosephosphate isomerase, Protein Eng. Des. Sel. 17 (2004) 375–382.
[38] K. Eaazhisai, H. Balaram, P. Balaram, M.R. Murthy, Structures of unliganded and inhibitor complexes of W168F, a Loop6 hinge mutant of plasmodium falciparum triosephosphate isomerase: observation of an intermediate position of loop6, J. Mol. Biol. 343 (2004) 671–684.
[39] X. Zhai, C.J. Reinhardt, M.M. Malabanan, T.L. Amyes, J.P. Richard, Enzyme architecture: amino acid side-chains that function to optimize the basicity of the active site glutamate of triosephosphate isomerase, J. Am. Chem. Soc. 140 (2018) 8277–8286.
[40] X. Zhai, T.L. Amyes, J.P. Richard, Role of loop-clamping side chains in catalysis by triosephosphate isomerase, J. Am. Chem. Soc. 137 (2015) 15185–15197.
[41] S. Choi, A.C. Hedman, S. Sayedyahossein, N. Thapa, D.B. Sacks, R.A. Anderson, Agonist-stimulated phosphatidylinositol-3,4,5-trisphosphate generation by scaffolded phosphoinositide kinases, Nat. Cell Biol. 18 (2016) 1324–1335.
[42] J.A. Silverman, R. Balakrishnan, P.B. Harbury, Reverse engineering the (beta/alpha)8 barrel fold, Proc. Natl. Acad. Sci. U. S. A. 98 (2001) 3092–3097.
[43] C.A. Reyes-Lopez, E. Gonzalez-Mondragon, C.G. Benitez-Cardoza, M.E. Chanez-Cardenas, N. Cabrera, R. Perez-Montfort, A. Hernandez-Arana, The conserved salt bridge linking two C-terminal beta/alpha units in homodimeric triosephosphate isomerase determines the folding rate of the monomer, Proteins 72 (2008) 972–979.
[44] J.P. Richard, X. Zhai, M.M. Malabanan, Reflections on the catalytic power of a TIM-barrel, Bioorg. Chem. 57 (2014) 206–212.
[45] J.P. Richard, Acid-base catalysis of the elimination and isomerization reactions of triose phosphates, J. Am. Chem. Soc. 106 (1984) 4926–4936.
[46] J.R. Knowles, Enzyme catalysis: not different, just better, Nature 350 (1991) 121–124.
[47] J.P. Richard, A paradigm for enzyme-catalyzed proton transfer at carbon: triosephosphate isomerase, Biochemistry 51 (2012) 2652–2661.
[48] R.C. Davenport, P.A. Bash, B.A. Seaton, M. Karplus, G.A. Petsko, D. Ringe, Structure of the triosephosphate isomerase-phosphoglycolohydroxamate complex: an analogue of the intermediate on the reaction pathway, Biochemistry 30 (1991) 5821–5826.
[49] A.J. Conway, F.C. Brown, E.J. Hortle, G. Burgio, S.J. Foote, C.J. Morton, S.M. Jane, D.J. Curtis, Bone marrow transplantation corrects haemolytic anaemia in a novel ENU mutagenesis mouse model of TPI deficiency, Dis. Model. Mech. 11 (2018).
[50] B. Holkova, S. Grant, Proteasome inhibitors in mantle cell lymphoma, Best Pract. Res. Clin. Haematol. 25 (2012) 133–141.
[51] T.A. Guerrero-Garcia, S. Gandolfi, J.P. Laubach, T. Hideshima, D. Chauhan, C. Mitsiades, K.C. Anderson, P.G. Richardson, The power of proteasome inhibition in multiple myeloma, Expert Rev. Proteomics 15 (2018) 1033–1052.
[52] E.E. Manasanch, R.Z. Orlowski, Proteasome inhibitors in cancer therapy, Nat. Rev. Clin. Oncol. 14 (2017) 417–433.
[53] S.M. Lewis, B.J. Bain, I. Bates, J.V. Dacie, J.V. Dacie, Dacie and Lewis Practical Haematology, 10th ed., Churchill Livingstone/Elsevier, Philadelphia, 2006.
[54] E. Beutler, Red Cell Metabolism: A Manual of Biochemical Methods, 3rd ed., Grune & Stratton, Orlando, FL, 1984.

[55] J. Huang, W. Zhou, W. Dong, A.M. Watson, Y. Hong, From the cover: directed, efficient, and versatile modifications of the Drosophila genome by genomic engineering, Proc. Natl. Acad. Sci. U. S. A. 106 (2009) 8284–8289.
[56] B. Ganetzky, C.F. Wu, Indirect suppression involving behavioral mutants with altered nerve excitability in drosophila melanogaster, Genetics 100 (1982) 597–614.
[57] F.W. Studier, Protein production by auto-induction in high density shaking cultures, Protein Expr. Purif. 41 (2005) 207–234.
[58] Z. Otwinowski, W. Minor, Processing of X-ray diffraction data collected in oscillation mode, Methods Enzymol. 276 (1997) 307–326.
[59] P. Emsley, B. Lohkamp, W.G. Scott, K. Cowtan, Features and development of coot, Acta Crystallogr. D Biol. Crystallogr. 66 (2010) 486–501.
[60] I.W. Davis, A. Leaver-Fay, V.B. Chen, J.N. Block, G.J. Kapral, X. Wang, L.W. Murray, W.B. Arendall 3rd, J. Snoeyink, J.S. Richardson, D.C. Richardson, MolProbity: all-atom contacts and structure validation for proteins and nucleic acids, Nucleic Acids Res. 35 (2007) W375–W383.
[61] F.H. Niesen, H. Berglund, M. Vedadi, The use of differential scanning fluorimetry to detect ligand interactions that promote protein stability, Nat. Protoc. 2 (2007) 2212–2221.